R. & M. No. 2773
(13,001)
A.R.C. Technical Report

MINISTRY OF SUPPLY

AERONAUTICAL RESEARCH COUNCIL
REPORTS AND MEMORANDA

Flow Patterns in the Wake of an Oscillating Aerofoil

By

J. B. BRATT, B.A., B.Sc.,
of the Aerodynamics Division, N.P.L.

LONDON: HER MAJESTY'S STATIONERY OFFICE
1953
PRICE 7s. 6d. NET

Flow Patterns in the Wake of an Oscillating Aerofoil

By

J. B. BRATT, B.A., B.Sc.,
of the Aerodynamics Division, N.P.L.

*Reports and Memoranda No. 2773**
March, 1950

Summary.—Part I of the report gives an account of experiments made with the National Physical Laboratory smoke generator to obtain smoke patterns in the wake of an aerofoil performing a rolling oscillation in a wind stream.

Calculations are given in Part II relating to the smoke patterns produced by a nozzle in uniform motion relative to (a) an infinite row of equally spaced two-dimensional discrete vortices of alternate sign and (b) an infinite two-dimensional vortex sheet with sinusoidal distribution of strength. Comparison with certain of the smoke patterns discussed in Part I suggests that the wake vorticity can be treated very closely as a system of discrete vortices, and this is supported by the consideration that the elements of a continuous vortex sheet would in general be subject to normal induced velocities, which would tend to break the sheet up. The tendency for this to occur would be greater for the higher values of ω, wince the variation of vorticity with distance along the wake would be greater. The induced velocities for a uniform infinite vortex sheet would be zero.

On the assumption that the theoretical infinite vortex sheet in the wake of an oscillating aerofoil breaks up into discrete vortices, the size of the vortex cores is calculated by satisfying the energy equation relating the two systems.

PART I

Experimental Flow Patterns

1. *Introduction.*—A knowledge of the flow pattern in the wake of an oscillating body such as an aerofoil or a control surface is of value in work on flutter and stability as a check on the theoretical assumptions made in estimating the aerodynamic forces on the body. It is also possible to estimate the circulation experimentally from quantitative measurements of the flow in the wake, and this information might then be used to determine certain of the forces. For example, a knowledge of the energy of circulation in the wake, together with the change in mean drag due to oscillation, would enable the damping to be determined.

Visualisation of air flow by means of smoke is now an established technique for static conditions (*e.g.*, determination of transition points on a stationary aerofoil), and a considerable amount of work has been done by Valensi[1] on the development of methods for the detailed examination of unsteady flow. The experiments described in the present paper were carried out to explore the possibility of examining the flow behind an oscillating aerofoil by means of a technique similar to that developed by Valensi. The main requirements of this technique are

(a) the generation of a suitable smoke,
(b) illumination of the smoke pattern,
(c) instantaneous photography of the smoke pattern.

* Published with the permission of the Director, National Physical Laboratory.

With regard to (a) it was decided to use the N.P.L. smoke generator (R. & M. 2023[2]), which had proved satisfactory in other work. Two possibilities exist in relation to (b) and (c). The smoke pattern can be illuminated continuously by means of a high intensity lamp (searchlight), short exposure photographs being taken with a camera of conventional type. Alternatively the source of illumination can be a discharge tube giving a high intensity flash of very short duration, in which case a camera without a high-speed shutter is used. This method was used by Valensi and has been adopted in the present tests on account of a number of advantages. Since the ultimate aim is a complete time record of unsteady flow, continuous lighting requires the use of a high-speed ciné camera, whereas with the flashing lamp a much simpler camera with a continuously moving film can be used, the flashes being controlled by the film drive. The high intensity flash is more efficient than continuous lighting since illumination takes place only whilst the photograph is being taken. The method is also more convenient, since for the same intensity of illumination the lamp is much smaller than with continuous lighting. If the flashing lamp is controlled by a variable-frequency oscillator, the apparatus can be used for stroboscopic observation of periodic phenomena.

All photographs taken during the tests described in this paper were single-flash exposures.

2. *General Arrangement of Apparatus.*—The tests followed a series of derivative measurements for decaying oscillations in roll made on a set of rigid aerofoils. A detailed description of the apparatus used in the derivative tests has been given in a previous report (R. & M. 2032[3]). Fig. 1 shows the main features of this apparatus with the additions required for maintaining an oscillation of constant amplitude.

A rectangular symmetrical NACA aerofoil (0015) of 20 in. chord and 60 in. span was used, hinged at the root chord to give freedom in roll. It was connected to helical springs above and below the tunnel by means of vertical wires attached at a point on the inertia axis 40 in. from the root chord. These wires were protected from wind forces by streamlined tubes. The wire passing through the roof of the tunnel was also attached to a horizontal steel arm pivoted at its mid-point and carrying masses for adjustment of frequency. Maintained oscillations were produced by means of a simple electrical self-exciting system constructed with components to hand. This method was preferred to inexorable mechanical forcing since a suitable mechanical oscillator was not available at the time.

The electrical driving system was formed by a coil S (Fig. 1) clamped to one end of the steel arm and situated in the field of a pot magnet P. A contact K at the opposite end of the arm closed momentarily when the coil reached its maximum upward displacement and energised the system through the circuit shown in Fig. 2. The action of this circuit was as follows. When K closed the two high-speed relays A, B operated and current flowed through the coils via the contacts B_1. The relays continued to hold in for some time after K had opened, since current flowed through their windings via the contacts A_1 from the charged condenser C. By adjustment of the time constant CR it was possible to make the relays hold in until the coil had reached its maximum downward displacement. Thus if the coil was connected in the correct sense, the reaction always assisted the motion. By this means quite powerful excitation could be obtained.

2.1. *Introduction of Smoke into Wind Stream.*—The N.P.L. smoke generator produces a dense fog of oil droplets by condensation of heated oil vapour, which passes through a small orifice into a current of cool air from a blower. This smoke can be fed conveniently to distant points through rubber tubing. In the initial tests this tubing entered the tunnel upstream of the honeycomb and was connected to a horizontal metal tube which passed through the honeycomb and terminated in a nozzle at a point in the tunnel contraction. Various positions in the contraction were tried, both with flat and circular nozzles, but in all cases, excepting at very low speeds, the smoke filament had become unstable and had dispersed by the time it reached the working section. At wind speeds of the order of 1 ft/sec a clean filament could be obtained with difficulty by very careful adjustment of the speed with which the smoke emerged from the nozzle.

The method finally adopted was that used by Valensi, in which the nozzle is situated in the working-section of the tunnel a short distance upstream of the model. The arrangement for two nozzles is indicated in Fig. 3. Smoke from the generator entered the tunnel through streamlined metal tubes T_1, T_2 which terminated in nozzles N_1, N_2 formed of short lengths of tube or circular cross-section with the ends remote from the model plugged and rounded. Details of the nozzle are given in Fig. 4. The junction of the streamlined tube and nozzle was faired with Plasticine, and the open end of the nozzle was filed from the inside to give a sharp edge. Vibration was prevented by means of stay wires as indicated in Fig. 3.

The best smoke filament is obtained when the smoke emerges from the nozzle with the local wind velocity. With the N.P.L. smoke generator and the nozzles described, the maximum speed for which this condition could be satisfied was about 40 ft/sec.

2.2. *Illumination of Smoke Pattern.*—The arrangement of the source of light L in relation to the smoke pattern M and camera or observation point N, for maximum intensity of image, is shown in Fig. 5. A screen O prevented direct rays from the lamp reaching the camera lens. The background was painted dead black.

Ample illumination for visual observation could be obtained with a small searchlight rated at 1400 watts. However, an experimental high-intensity discharge lamp provided by the research department of the General Electric Company was used. This lamp was in the form of a straight glass tube approximately 0·25 of an inch in external diameter with electrodes sealed into the ends at a distance of about 6 in. apart. The tube contained Krypton at low pressure, and a triggering electrode consisting of a wire inside a glass tube of small bore was attached to the outside of the lamp.

The energising circuit for the lamp is illustrated in Fig. 6. Condensers C and C_1 were charged to a high voltage through the resistances R and R_1. By means of the high-speed relay D the condenser C_1 was discharged through the primary winding of an ignition coil I to produce a high voltage pulse on the triggering electrode T connected to the secondary winding. The resultant ionisation in the lamp rendered the latter conducting, and the condenser C immediately discharged through the lamp to give a high-intensity flash of approximately 5 microseconds duration. The relay D could be operated by a remote switch for single flash work, or alternatively it could be energised from the aerofoil driving circuit to give flashes synchronised with the motion of the aerofoil at the rate of one flash per cycle. With the latter mode of operation it was necessary for the time constants RC, RC_1 to be small compared with the time interval between flashes. The condenser C had a capacity of $12\mu F$ and was charged to 1400 volts, which corresponds to an energy input to the lamp of 12 Joules per flash.

A reflector consisting of a sheet of aluminium bent to an approximate parabolic form was used to concentrate the light from the lamp on to the smoke pattern.

3. *Photographs of Flow.*—Figs. 7 to 15 show illustrative single-flash exposures. In all cases where the aerofoil appears in the photograph the trailing edge and part of the lower surface of the aerofoil are visible, the root chord being concealed in the background. The direction of the wind is from right to left.

The notation employed in the figures is as follows.

f denotes frequency in cycles/sec

V ,, wind speed in ft/sec

ω ,, the non-dimensional frequency parameter defined by

$$\omega = \frac{2\pi fc}{V}$$

where c is the chord in feet.

Nozzle positions are given in the table below, where D is the distance of the plane of the nozzle from the wing tip measured towards the root, d the distance of the mouth of the nozzle upstream from the leading edge of the aerofoil, and h the distance of the nozzle above or below the chord line of the stationary aerofoil in its mean position, all dimensions being in inches. These positions are also indicated in Fig. 22.

Position	D	d	h
1	32	10	2 (below)
2	32	14	1 ,,
3	32	14	3 (above)
4	15	10	1 (below)

With the aerofoil oscillating, the flow was disturbed for some distance ahead of the leading edge, so that the smoke filament emerging from the mouth of the nozzle immediately indicated a wave-like motion. The smoke pattern in the wake appeared to be independent of the distance of the nozzle upstream of the aerofoil within the range 10 to 20 in. covered in the tests.

Estimates of the speed with which the smoke pattern travelled downstream were obtained from measurements of the photographic records and the known geometry and frequency of the system. The ratio of this to the free stream velocity was found to be unity at very low tunnel speeds, but decreased as the latter increased, a value of 0·7 being obtained for a wind speed of 16 ft/sec. This effect is presumably due to loss of momentum in the wake arising from drag.

The mean incidence and amplitude of oscillation relating to the photographs discussed below were 0 deg and 0·75 deg respectively.

The term vortex used in the following descriptions of the flow photographs is intended to describe only the form of the smoke trace and must not be taken to imply the presence of discrete vortices in the flow itself (*see* Part II).

3.1. *Variation of Flow Pattern with* ω.—The photographs in Fig. 7 show the change in flow pattern as the wind speed was raised from 2·6 to 35·5 ft/sec, the frequency being maintained at 4·26 c.p.s. This corresponds to a variation of ω from 17 to 1·3. At the lowest wind speed (Fig. 7, No. 1) very clear and distinct vortices were obtained, which grew in size as they travelled downstream. When viewed with continuous light the cores of these vortices were seen to be spiralling out in a spanwise direction from root to tip. Observation with synchronised flashes was very impressive, the smoke pattern appearing perfectly stationary with the exception of the vortex cores, into which the smoke penetration varied with time. The smoke filament, however, always appeared to run along exactly the same spiral in space. With increasing wind speed (reduction in ω) the vortices became more separated and less distinct until finally they disappeared leaving a wave-like smoke pattern of which the amplitude decreased and the wavelength increased with further increase in wind speed (Fig. 7, Nos. 3 to 5).

The initial stages in the formation of the vortices could be observed clearly at the trailing edge. In Fig. 7, No. 1, the peak immediately behind the trailing edge was formed by the smoke filament being thrown upwards following the motion of the aerofoil. An instant later this peak burst into two vortices spinning in opposite senses, one on each side. The beginning of this process can be seen in Fig. 12, No. 3.

The fine structure appearing in the smoke filament at the higher wind speeds was thought to be due to eddies shed from the nozzle and possibly from the model as well.

3.2. *Nozzles Above and Below Level of Model.*—Fig. 8 relates to the same frequency and range of wind speed as Fig. 7, but only three values of wind speed were used. Exposures 1 to 3 were obtained with a single nozzle 1 in. below the mean position of the chord line. Exposures 4 to 6

are repeats of Nos. 1 to 3 in relation to wind speed but an additional nozzle was placed 3 in. above the mean position of the chord line. The non-symmetrical arrangement of the two nozzles as related to the position of the model was essential for obtaining two equally distinct smoke filaments at the lowest wind speed. This was thought to be due to asymmetric flow in the tunnel.

Exposure 4 shows the interlacing of the smoke filaments in the vortex pattern, and this is seen again in Fig. 9, No. 2. Exposures 1 and 3 in Fig. 9 were obtained with the separate lower and upper nozzles respectively.

3.3. *Flow Pattern at Low Frequency and Wind Speed.*—The somewhat curious pattern shown in Fig. 10 was obtained at a wind speed of 1·10 ft/sec and a frequency of 0·75 c.p.s. The velocity distribution in the tunnel at this low wind speed was extremely bad and varied with time, which probably explains why the pattern could not be repeated later. The lower wind speeds were measured with a vane anemometer.

3.4. *Comparison of Flow at Two Points Along Span.*—Exposures 1 to 3 in Fig. 11 accord with Nos. 1 to 3 in Fig. 8 and refer to a position roughly half-way along the span. Exposures 4 to 6 in Fig. 11 relate to the same wind speeds and frequency as Nos. 1 to 3, but the nozzle lay one-quarter of the span inboard from the tip. The most marked difference is apparent at the lowest wind speed (Nos. 1 and 4), the vortices for the position nearer the tip growing more rapidly than for the mid-span position and quickly breaking up.

An attempt was made to show tip vortices by placing the nozzle 2 in. inboard from the tip, but the smoke dispersed rapidly and no definite vortices were observed. No photographs were taken.

3.5. *Variation of Flow Pattern with* ω.—The series in Fig. 12 is similar to that in Fig. 7, but begins at a much higher value of ω, the range being from 46 to 3·6. In exposure No. 1 a single vortex is seen forming at the trailing edge, but the vortices in the wake were so crowded and distorted as to give the appearance of a diffuse cloud of smoke. A pair of vortices is just faintly visible following the vortex at the trailing edge in exposure No. 1. With increase in wind speed the vortices in the wake began to separate out, as seen in exposure No. 2, where the first vortex pair is completely formed. Further increase in wind speed (Nos. 3 to 6) gave clearly defined vortices which finally disappeared in the manner described in Fig. 7.

3.6. *Comparison of Flow for Two Values of Frequency.*—Exposures 1 to 3 in Fig. 13 relate to a frequency of 1·7 c.p.s., and Nos. 4 to 6 to a frequency of 5·72 c.p.s. The latter three exposures are identical with Nos. 4 to 6 in Fig. 12. Wind speeds were adjusted to give roughly equal values of ω for corresponding exposures in the two groups. For example, Nos. 1 and 4 had values of ω equal to 16 and 14 respectively. It will be observed that the flow pattern was identical in these two cases although the frequencies differed by a factor of approximately 3·4. This indicates that for these particular tests the flow pattern depends primarily on ω. The flow patterns in the other pairs of photographs also correspond well, although the agreement is not so good as in Nos. 1 and 4.

This may be due to the greater difference between the corresponding values of ω, which was difficult to set accurately to a required value at low wind speeds.

3.7. *Aerofoil Stationary.*—For the photographs in Fig. 14 the wind speed ranged from 2·6 to 120 ft/sec. Small vortices were observed at the lowest wind speed (No. 1), but these seemed very unstable, and rapidly broke up. It is of interest to note that at the highest wind speed of 120 ft/sec (No. 4) a smoke filament of sufficient density for photography was obtained in spite of the fact that the maximum speed of efflux of the smoke from the nozzle was approximately 40 ft/sec with the existing smoke generator.

3.8. *Aerofoil Removed from Tunnel.*—These tests were made in order to determine whether the irregularities appearing in the smoke filament at the higher wind speeds were due solely to the model. It is clear from Fig. 15 that this was not the case, since a large amount of fine structure is visible at speeds above 2·6 ft/sec. An additional test was made at 2·6 ft/sec with the streamlined tubes for guarding the wires removed.

The smoke filament obtained was almost identical with that seen in exposure No. 2, which indicates that the tubes had little influence on the flow in the region of the pattern.

PART II

Calculations Relating to Flow in the Wake

4. *Introduction.*—The second part of this report is concerned with some elementary theoretical calculations relating to flow behind an oscillating aerofoil. Although the conditions assumed are somewhat remote from those applying in the first part of the report, the treatment may help in the interpretation of the smoke traces.

In accordance with two-dimensional vortex-sheet theory, an oscillating aerofoil in uniform motion relative to the air at infinity leaves in its wake a linear sheet of vorticity, the strength of which varies sinusoidally with distance along the wake. It is assumed in the theory that this sheet extends to infinity behind the aerofoil; it is easily seen, however, that such a system must be unstable as a result of the action of induced velocities. In part of the following analysis it is assumed that the sheet breaks up into a single row of equidistant discrete cortices of alternate sign.

For simplicity the vortex system is treated as stationary, and the nozzle is regarded as moving uniformly relative to the system. The instantaneous smoke trace is clearly identical with that obtained when the vortices move and the nozzle is stationary, as for the experiments described in Part I. The formulae derived enable the smoke trace at any instant to be plotted for the case of a nozzle moving with uniform velocity parallel to (a) an infinite row of equal transverse line vortices of alternate sign, and (b) an infinite vortex sheet with sinusoidal distribution of strength. Both cases might be regarded as relating to conditions at a great distance behind an oscillating aerofoil.

The row of discrete vortices (a) forms a system in neutral equilibrium*, and thus might be expected to persist for a certain length of time; the system is necessarily a mathematical abstraction, however, since it implies an infinite increment of energy in the wake per cycle for unit span. It will be obvious that the energy equation for the continuous and the discrete vortex systems can be reconciled by assuming the vorticity in the latter to be distributed in cores of finite size, the flow outside the cores remaining unaltered. On the assumption that these cores behave effectively as circular cylinders rotating bodily about their centres, a value for the diameter is obtained.

5. *Smoke Pattern for an Infinite Row of Discrete Vortices.*—5.1. *Equation of Streamlines.*—Consider an infinite row of equal two-dimensional line vortices equally spaced along the x-axis of a co-ordinate system, one of the vortices being at the origin. It may be shown† that the

* The induced velocity at any vortex is zero. This is easily seen by considering the effect of the remaining vortices taken in pairs equidistant from the vortex. The instability resulting from small displacements is proved in Ref. 4, p. 423.

† Ref. 4, p. 416.

velocity potential w for such a system is given by

$$w = -ik \log_e \sin \frac{\pi z}{a},$$

$$= -ik \log \sin (X + iY), \quad .. \quad .. \quad .. \quad .. \quad .. \quad .. \quad .. \quad (1)$$

where $X = \frac{\pi x}{a}$,

$Y = \frac{\pi y}{a}$,

a = spacing of vortices,

$k = \frac{K}{2\pi}$,

K = vortex strength (positive for anticlockwise circulation).

Equation (1) may be written

$$w = \phi_+ + i\psi_+ = -ik \log (\sin X \cosh Y + i \cos X \sinh Y), \quad .. \quad .. \quad (2)$$

and equating imaginary parts gives

$$\psi_+ = -\tfrac{1}{2}k \log \tfrac{1}{2}(\cosh 2Y - \cos 2X), \quad .. \quad .. \quad .. \quad .. \quad .. \quad (3)$$

where ψ_+ is the stream function for an infinite set of positive vortices*. The corresponding functions ψ_- for a set of equally storng negative vortices displaced a distance $a/2$ along the x-axis relative to the positive set is obtained from (3) by the substitution k for $-k$, x for $x + a/2$. Thus

$$\psi_- = \tfrac{1}{2}k \log \tfrac{1}{2}(\cosh 2Y + \cos 2X). \quad .. \quad .. \quad .. \quad .. \quad .. \quad .. \quad (4)$$

It follows that the stream function ψ for an infinite set of alternately positive and negative vortices of equal strength and uniform spacing $a/2$ is given by

$$\psi = \psi_+ + \psi_- = \tfrac{1}{2}k \log \frac{\cosh 2Y + \cos 2X}{\cosh 2Y - \cos 2X}. \quad .. \quad .. \quad .. \quad .. \quad .. \quad (5)$$

Equation (5) may be written in the simple form

$$\cos 2X = \tanh \frac{\psi}{k} \cosh 2Y. \quad .. \quad .. \quad .. \quad .. \quad .. \quad .. \quad .. \quad (6)$$

Streamlines may be plotted with the aid of (6) by calculation of corresponding values of x and y for assigned values of ψ (*see* Fig. 16).

5.2. *Equations for Smoke Trace.*—Imagine a smoke nozzle moving with uniform velocity parallel to the x-axis through the system of streamlines shown in Fig. 16. As the nozzle crosses each streamline a particle of smoke will be left behind which will travel along the streamline with the local velocity at each point. The curve on which the smoke particles lie at some subsequent time is the required smoke trace.

The x-component u of the velocity at a point in the vortex field may be obtained from (6) and is given by

$$u = \frac{\partial \psi}{\partial y} = -\frac{\pi k}{a} \sinh \frac{2\psi}{k} \tanh 2Y. \quad .. \quad .. \quad .. \quad .. \quad .. \quad .. \quad (7)$$

* The factor 1/2 is omitted in the formula for ψ given in Ref. 4, p. 417.

Thus for motion of a particle along a streamline

$$\frac{dx}{dt} = -\frac{\pi k}{a} \sinh \frac{2\psi}{k} \tanh 2Y, \quad .. \quad .. \quad .. \quad .. \quad .. \quad .. \quad .. \quad (8)$$

where x relates to position on the streamline and ψ is constant. If the nozzle leaves a smoke particle at a position x_1, its position x after a time t has elapsed is given by the relation

$$t = -\frac{a}{\pi k \sinh \frac{2\psi}{k}} \int_{x_1}^{x} \frac{dx}{\tanh 2Y}. \quad .. \quad .. \quad .. \quad .. \quad .. \quad .. \quad .. \quad (9)$$

Substitution from (6) and change of independent variable to X leads then to

$$\pm \frac{2\pi^2}{a^2} kt \sinh \frac{2\psi}{k} = \sin^{-1}\left(\frac{\sin 2X}{\operatorname{sech} \frac{\psi}{k}}\right) - \sin^{-1}\left(\frac{\sin 2X_1}{\operatorname{sech} \frac{\psi}{k}}\right), \quad .. \quad .. \quad .. \quad (10)$$

or say

$$\pm W = \theta - \theta_1. \quad .. \quad .. \quad .. \quad .. \quad .. \quad .. \quad .. \quad .. \quad .. \quad (11)$$

From (11)

$$\sin \theta = \sin \theta_1 \cos W \pm \cos \theta_1 \sin W, \quad .. \quad .. \quad .. \quad .. \quad .. \quad .. \quad (12)$$

which yields on use of (6), (10) and (11)

$$\sin 2X = \sin 2X_1 \cos W \pm \cos 2X_1 \sin W \tanh 2Y_1. \quad .. \quad .. \quad .. \quad (13)$$

The smoke trace is most conveniently plotted by taking the origin at each vortex in turn. Values of X_1 and Y_1 corresponding to points on streamlines encircling the vortex, at which smoke particles are left behind, are then selected and values of ψ determined from (6) (k is assumed known). Corresponding values of t, and hence W, for each X_1 are obtained from a knowledge of the speed and final position of the nozzle. Finally X and Y are determined from (13) and (6) respectively.

No ambiguity in the magnitude of X can arise since $x > a/4$. Ambiguity in sign in equations (10) to (13) and in the value of Y may be resolved with the aid of the diagrams in Fig. 17. These illustrate the correspondence between θ and the position P (x,y) of a particle on its streamline. It is readily shown with the aid of (6) that OR always lies in the same quadrant as OP, and since W represents a rotation from position θ_1 the quadrant containing P can be determined. From consideration of the direction of rotation it follows that when ψ is positive (anticlockwise rotation) the negative sign must be taken in equations (10) to (13), and vice versa.

5.3. *Values of k and a.*—If K_0 is the amplitude of the circulation about the aerofoil assumed to be producing the vortices, it is reasonable to suppose that the strength of each vortex is numerically equal to the change in circulation from its maximum negative to its maximum positive value. Thus

$$K = 2K_0 = 2\pi k. \quad .. \quad .. \quad .. \quad .. \quad .. \quad .. \quad .. \quad .. \quad .. \quad (14)$$

For a vertical translational oscillation of amplitude z_0, two-dimensional vortex-sheet theory gives

$$K_0 = \frac{4Vz_0}{F\left(\frac{\omega}{2}\right)}, \quad .. \quad .. \quad .. \quad .. \quad .. \quad .. \quad .. \quad .. \quad .. \quad (15)$$

where V and ω are as defined in Part I, and $F(\omega/2)$ is expressible in terms of Bessel functions by the relation

$$\left\{F\left(\frac{\omega}{2}\right)\right\}^2 = \left\{J_1\left(\frac{\omega}{2}\right) + Y_0\left(\frac{\omega}{2}\right)\right\}^2 + \left\{J_0\left(\frac{\omega}{2}\right) - Y_1\left(\frac{\omega}{2}\right)\right\}^2 . \quad .. \quad .. \quad .. \quad (16)$$

This result may be derived from information given in a paper by W. P. Jones (R. & M. 2124[5]). Thus

$$k = \frac{4Vz_0}{\pi F\left(\frac{\omega}{2}\right)} . \quad .. \quad .. \quad .. \quad .. \quad .. \quad .. \quad .. \quad .. \quad .. \quad (17)$$

Since the vortex array is regarded as stationary, the distance a between successive vortices of like sign must equal the distance travelled by the aerofoil per cycle, hence

$$a = \frac{V}{f} = \frac{2\pi c}{\omega} . \quad .. \quad .. \quad .. \quad .. \quad .. \quad .. \quad .. \quad .. \quad .. \quad (18)$$

6. *Smoke Pattern for an Infinite Vortex Sheet.*—6.1. *Equation of Streamlines.*—In this case an infinite two-dimensional vortex sheet is assumed to extend along the x-axis, the strength being a periodic function of x with wavelength a. If the vortex strength per unit length at a point x is given by the expression

$$\varkappa \cos \frac{2\pi x}{a} \quad .. \quad .. \quad .. \quad .. \quad .. \quad .. \quad .. \quad .. \quad .. \quad .. \quad (19)$$

the velocity potential for an infinite set of equal elements dr of the sheet with spacing a is obtained from (1) in the form

$$dw = -\frac{\varkappa}{2\pi} \log \sin \frac{\pi}{a}(z - r) \, . \cos \frac{2\pi}{a} r \, \mathrm{dr}, \quad .. \quad .. \quad .. \quad .. \quad .. \quad (20)$$

where r is the position of the element nearest to the origin. The velocity potential for the whole sheet is thus given by

$$w = -\frac{i\varkappa}{2\pi} \int_0^a \log \sin \frac{\pi}{a}(z - r) \cos \frac{2\pi}{a} r \, dr, \quad .. \quad .. \quad .. \quad .. \quad .. \quad (21)$$

$$= -\frac{i\varkappa a}{2\pi^2} \int_0^\pi \log \sin (Z - R) \cos 2R \, dR, \quad .. \quad .. \quad .. \quad .. \quad .. \quad (22)$$

where $R = (\pi/a)r$ and $Z = X + iY$ as defined in section 5.1, where Y may be small but is never zero.

Integration by parts leads to

$$\frac{2\pi^2 iw}{\varkappa a} = \tfrac{1}{2} \int_0^\pi \frac{\sin 2R \, dR}{\tan (Z - R)} \quad .. \quad .. \quad .. \quad .. \quad .. \quad .. \quad .. \quad (23)$$

$$= \tfrac{1}{2} \sin 2Z \int_0^\pi \frac{dR}{\tan (Z - R)} - \tfrac{1}{2} \cos 2Z \int_0^\pi dR - \tfrac{1}{2} \int_0^\pi \cos 2R \, dR. \quad .. \quad .. \quad (24)$$

The second and third integrals are π and 0 respectively. The first integral may be written

$$-\int_{R=0}^{\pi} \frac{d\{\sin (Z - R)\}}{\sin (Z - R)} = -\Big[\log | \sin (Z - R) | + i \arg \sin (Z - R)\Big]_0^\pi , \quad .. \quad (25)$$

and since the modulus of sin $(Z - R)$ is the same for $R = 0$ and π, only the change in argument need be considered. It is easily shown that

$$\arg \sin (Z - R) = \tan^{-1} \left\{ \tanh Y \tan \left(\frac{\pi}{2} - X + R \right) \right\}. \quad .. \quad .. \quad .. \quad (26)$$

Thus, when R goes from 0 to π the argument changes by $\pm \pi$, the positive sign corresponding to a positive Y and *vice versa*. Hence

$$\int_0^{\pi} \frac{dR}{\tan (Z - R)} = \mp i\pi, \quad .. \quad .. \quad .. \quad .. \quad .. \quad .. \quad .. \quad (27)$$

and therefore from (24)

$$\frac{2\pi^2 iw}{\varkappa a} = - \frac{\pi}{2} e^{\mp 2Y} (\cos 2X \pm i \sin 2X), \quad .. \quad .. \quad .. \quad .. \quad .. \quad (28)$$

in which the upper and lower signs correspond to positive and negative values of Y respectively. The stream function is then given by

$$\psi = \frac{\varkappa a}{4\pi} e^{-|2Y|} \cos 2X. \quad .. \quad .. \quad .. \quad .. \quad .. \quad .. \quad .. \quad .. \quad (29)$$

Streamlines calculated with the aid of (29) are shown in Fig. 18. The main feature of these is a discontinuity where each streamline crosses the x-axis.

6.2. *Equations for Smoke Trace.*—The x-component of the velocity at any point is given by

$$u = \frac{\partial \psi}{\partial y} = \mp \frac{\varkappa}{2} e^{-|2Y|} \cos 2X = \mp \frac{\varkappa}{2} \psi, \quad .. \quad .. \quad .. \quad .. \quad .. \quad (30)$$

thus for a given streamline u is of constant magnitude. If l is the x-component of the distance travelled by the smoke particle since leaving position x_1, y_1, then

$$l = | u | t, \quad .. \quad .. \quad .. \quad .. \quad .. \quad .. \quad .. \quad .. \quad .. \quad (31)$$

where t is the time elapsed. The motion takes place between limits $\pm |x_0|$, where $|x_0| \gtrless a/4$, and the corresponding quantity $|X_0|$ is obtained from (29) in the form

$$\cos 2X_0 = e^{-|2Y_1|} \cos 2X_1, \quad .. \quad .. \quad .. \quad .. \quad .. \quad .. \quad .. \quad (32)$$

the origin being at the centre of the streamline under consideration.

The value of X corresponding to the final position of the smoke particle is most readily obtained by considering the distance travelled on a diagram of the streamline (as indicated for x in Fig. 18). A formal solution is given by the expressions

$$L = X_1 + 2n|X_0| - (-1)^n X \quad .. \quad .. \quad .. \quad .. \quad .. \quad .. \quad .. \quad (33)$$

when ψY_1 is positive, and

$$L = - X_1 + 2n|X_0| + (-1)^n X \quad .. \quad .. \quad .. \quad .. \quad .. \quad .. \quad (34)$$

when ψY_1 is negative, where $L = \pi l/a$, n is a positive integer, and $|X| \gtrless |X_0|$.

The value of Y is then found with the aid of (29), the value of ψ having been previously determined by substitution of X_1 and Y_1. The sign of Y is given by $(-1)^n Y_1$.

6.3. *Values of $\varkappa$ and a.*—In this case the change in circulation $2K_0$ about the aerofoil corresponds to a production of vorticity in the wake equal to that between $x = -a/4$ and $+a/4$.

Thus

$$2K_0 = \varkappa \int_{a/4}^{a/4} \cos \frac{2\pi x}{a}\, dx = \frac{a\varkappa}{\pi}, \quad \ldots \quad (35)$$

and from section 5.3, for translational oscillation,

$$\varkappa = \frac{8\pi V z_0}{aF\left(\frac{\omega}{2}\right)}. \quad \ldots \quad (36)$$

The value of a is given by the same formula as in section 5.3.

7. *Calculated Smoke Traces.*—Traces are shown in Figs. 19 and 20 for both discrete and continuous vortex systems, the nozzle travelling along the x-axis in each case. The parameters selected for these calculations correspond to the case of a two-dimensional aerofoil performing a vertical translational oscillation for which $\omega = 17$, $c = 1{\cdot}67$ ft, $z_0 = 0{\cdot}1818$ ft, and $V = 2{\cdot}6$ ft/sec, the last being also the velocity of the nozzle. The values of ω, c, V agree with those of Fig. 7, No. 1, and a marked similarity of pattern is evident. The main difference is the arrangement of the vortices in the experimental trace in two slightly separated rows resembling a von Kármán street. The ratio of row to vortex spacing, however, is much smaller than for a stable von Kármán configuration.

A pattern similar to Fig. 7, No. 4 was calculated for a value of $\omega = 3{\cdot}6$, with the nozzle displaced from the x-axis. This is not included in the report, since it is of relatively minor interest.

The traces plotted in Figs. 19 and 20 spiral in to the centres of the systems of streamlines on which they are based; the central portions have been omitted, however, since the plotting becomes very troublesome in those regions. Similar traces have been obtained for a nozzle displaced from the x-axis, in which case the pattern spirals in to the streamlines to which the path of the nozzle forms a tangent.

Comparison of the traces for discrete and continuous vortex systems shows that the distinguishing feature is a discontinuity in the slope of the latter at each point where the trace crosses the x-axis. This arises from the discontinuous nature of the streamlines as seen from Fig. 18, which itself arises from the presence of the vortex sheet.

The absence of discontinuities in the smoke trace of Fig. 7, No. 1, may be taken as an argument in favour of the discrete vortex system. It is felt, however, that such evidence is unsatisfactory, especially since large discontinuities of slope would be expected only near the centres of the streamline system. Convincing evidence could be obtained from a knowledge of the distribution of vorticity over the field, which necessitates being able to estimate the circulation around any closed path. This can only be done if the vector velocity at each point is known. It appears that the only way in which this information can be obtained is by photographic recording of the motion of a large number of discrete particles introduced into the field.

8. *Energy Relations in the Wake.*—8.1. *Kinetic Energy Increments for a Discrete Vortex System.*—In the treatment which follows the discrete vortices discussed in section 5.1 are assumed to possess cylindrical cores of radius s, and to rotate bodily about their centres. The increment of kinetic energy E per cycle in the wake of an aerofoil producing this system is given by

$$E = \tfrac{1}{2}\rho \int_{-\infty}^{\infty} \int_{a/4}^{a/4+a} (u^2 + v^2)\, dx\, dy, \quad \ldots \quad (37)$$

where u and v are the x- and y-components of velocity and ρ is density.

External to the cores

$$u^2 + v^2 = u\frac{\partial \psi}{\partial y} - v\frac{\partial \psi}{\partial x}$$

$$= -\frac{\partial(v\psi)}{\partial x} + \frac{\partial(u\psi)}{\partial y} \quad .. \quad .. \quad .. \quad .. \quad .. \quad .. \quad .. \quad (38)$$

since the flow is irrotational. Thus the corresponding energy increment E_e is by Stokes' theorem given by

$$E_e = -\tfrac{1}{2}\rho \iint \left\{ \frac{\partial(v\psi)}{\partial x} - \frac{\partial(u\psi)}{\partial y} \right\} dx\, dy$$

$$= -\tfrac{1}{2}\rho \oint (u\psi\, dx + v\psi\, dy), \quad .. \quad .. \quad .. \quad .. \quad .. \quad .. \quad .. \quad (39)$$

where the path of integration is as indicated in Fig. 21. The integral around the outer boundary is clearly zero since ψ vanishes here. Thus

$$E_e = \rho \int_C (u\psi\, dx + v\psi\, dy) \quad .. \quad .. \quad .. \quad .. \quad .. \quad .. \quad .. \quad (40)$$

where C denotes integration round the circumference of one core taken anticlockwise. For convenience this is taken at the origin, since the integral (40) would be the same for any core.

It follows from equation (5) that

$$\psi = \tfrac{1}{2}k \log \frac{1 + \sinh^2 Y - \sin^2 X}{\sinh^2 Y + \sin^2 X}$$

$$\simeq \tfrac{1}{2}k \log \frac{1}{Y^2 + X^2}$$

if X and Y are small. Hence on the circumference of the core

$$\psi = k \log \frac{a}{\pi s}. \quad .. \quad .. \quad .. \quad .. \quad .. \quad .. \quad .. \quad .. \quad .. \quad (41)$$

Thus

$$E_e = \psi\rho \int_C (u\, dx + v\, dy)$$

$$= 2\pi\rho k^2 \log \frac{a}{\pi s}. \quad .. \quad .. \quad .. \quad .. \quad .. \quad .. \quad .. \quad .. \quad .. \quad (42)$$

The energy for the cores E_c is given by

$$E_c = \tfrac{1}{2}\pi\rho k^2, \quad .. \quad .. \quad .. \quad .. \quad .. \quad .. \quad .. \quad .. \quad .. \quad (43)$$

which follows immediately from the angular velocity in terms of circulation, and the area. Thus

$$E = E_e + E_c$$

$$= \frac{\rho K_0^2}{\pi}\left(\tfrac{1}{2} + 2 \log \frac{a}{\pi s}\right) \quad .. \quad .. \quad .. \quad .. \quad .. \quad .. \quad .. \quad (44)$$

from equation (14).

8.2. *Kinetic Energy Increments for a Continuous Vortex System.*—In this case the system considered is that of section 6.1, and from equation (29) it follows that

$$u^2 + v^2 = \left(\frac{\partial \psi}{\partial y}\right)^2 + \left(\frac{\partial \psi}{\partial x}\right)^2$$

$$= \frac{\varkappa^2}{4} e^{-|4Y|} \quad .. \quad .. \quad .. \quad .. \quad .. \quad .. \quad .. \quad .. \quad (45)$$

Thus

$$E = \rho a \int_0^\infty \frac{\varkappa^2}{4} e^{-|4Y|}\, dy$$

$$= \frac{\pi \rho K_0^2}{4} \quad .. \quad .. \quad .. \quad .. \quad .. \quad .. \quad .. \quad .. \quad .. \quad (46)$$

from equation (35).

8.3. *Radii of the Vortex Cores.*—Since there should be ideally no change in kinetic energy if a continuous system of vorticity breaks up into discrete vortices, an equation for s can be obtained by equating the expressions for E derived in the two preceding sections. Thus

$$\rho \frac{K_0^2}{\pi} \left(\tfrac{1}{2} + 2 \log \frac{a}{\pi s}\right) = \frac{\pi \rho K_0^2}{4},$$

which leads to

$$\log \frac{a}{\pi s} = \frac{\pi^2 - 2}{8}, \quad .. \quad .. \quad .. \quad .. \quad .. \quad .. \quad .. \quad .. \quad .. \quad (47)$$

whence

$$s = a/8{\cdot}401. \quad .. \quad .. \quad .. \quad .. \quad .. \quad .. \quad .. \quad .. \quad .. \quad (48)$$

Hence the ratio of s to a is a constant. The system of vortex cores is plotted to scale in Fig. 21.

Some idea of the degree of approximation involved in equation (41) may be obtained by substitution of the above value of s to give a value of ψ/k, which, with the aid of (6), gives the shape of the corresponding streamline. The major axis is found to be 5 per cent greater and the minor axis 5 per cent less than the diameter of the circular core.

9. *Conclusions.*—The similarity of the calculated smoke traces to the experimental trace of Fig. 7, No. 1, suggests that the assumed distributions of vorticity in the wake are possible. The question as to whether the discrete or continuous vortex system is a better representation of the actual flow pattern is difficult to answer, but it is clear from Fig. 18 that in the infinite continuous sheet all the vortex elements excepting those at the centres of the streamline system are subject to induced velocities, with the result that the sheet must ultimately break up.

In Fig. 7, No. 1, smoke particles have passed through the position which would be occupied by a vortex sheet and have already attained quite large transverse displacements close to the trailing edge of the aerofoil. This suggests that for large values of ω the vortex sheet breaks up rapidly.

A detailed knowledge of the flow around the profile and in the wake of an oscillating aerofoil is regarded as a matter of considerable importance, since it affects the basic assumptions of derivative theory. It is hoped that further information will be obtained from tests to be made in the N.P.L. water tunnel.

Acknowledgements.—Acknowledgements are due to Mr. C. J. Davis and Miss C. M. Luff, formerly of the Aerodynamics Division, N.P.L., for assistance in the experimental work and computation respectively, and also to Professor J. Valensi of the Institute of Fluid Mechanics, Marseilles, for valuable advice in connection with the design and use of smoke nozzles.

REFERENCES

No.	*Author*	*Title, etc.*
1	J. Valensi	Etude de l'écoulement de l'air autour d'une hélice. Publications Scientifique et Technique du Ministère de l'Air. No. 73.
2	J. H. Preston and N. E. Sweeting..	An Improved Smoke Generator for use in the Visualisation of Airflow particularly Boundary Layer Flow at High Reynolds Numbers. R. & M. 2023. October, 1943.
3	J. B. Bratt and C. J. Davis ..	The Influence of Aspect Ratio and Taper on the Fundamental Damping Derivative Coefficient for Flexural Motion. R. & M. 2032. February, 1945.
4	L. Bairstow	*Applied Aerodynamics* (Second Edition). Longmans, Green & Co.
5	W. P. Jones	Theoretical Air-load and Derivative Coefficients for Rectangular Wings. R. & M. 2124. February, 1943.

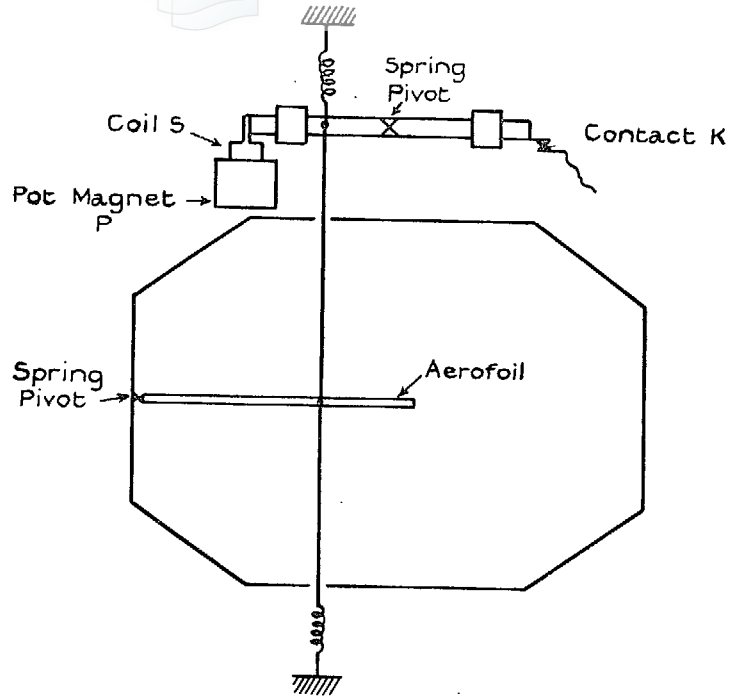

FIG. 1. General arrangement of apparatus.

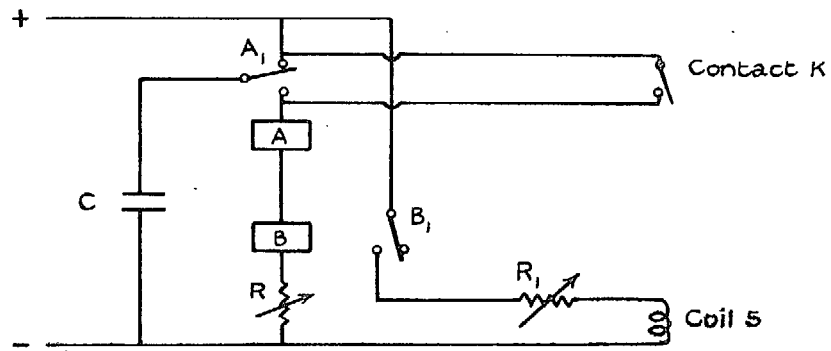

FIG. 2. Exciting circuit.

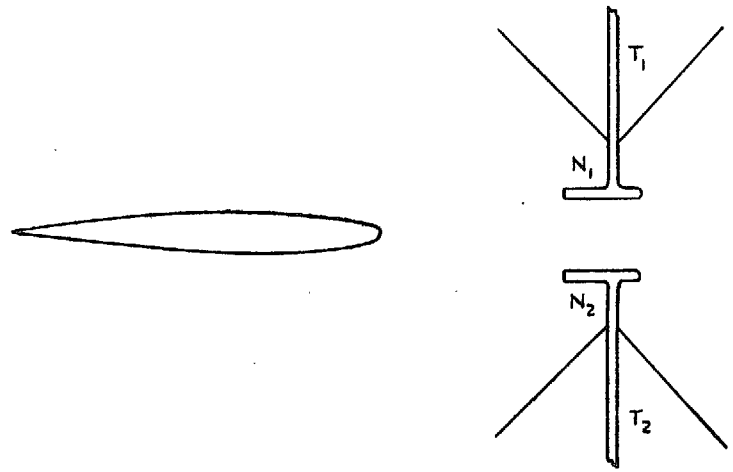

FIG. 3. Arrangement for two nozzles.

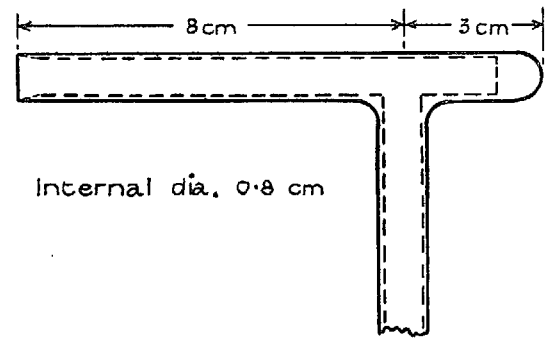

FIG. 4. Details of nozzle.

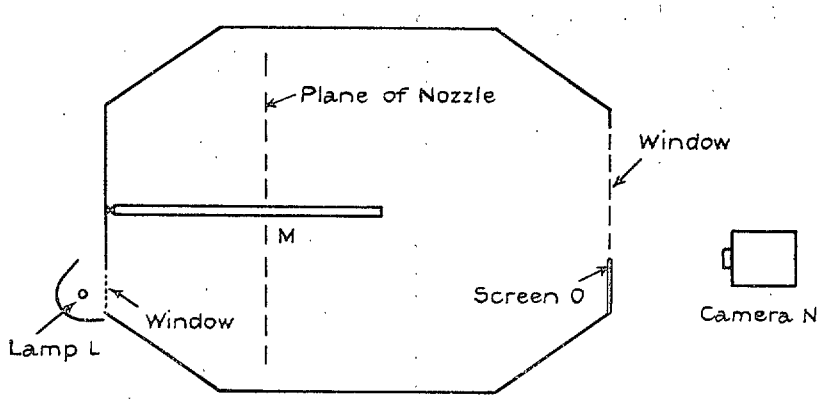

FIG. 5. Illumination of smoke pattern.

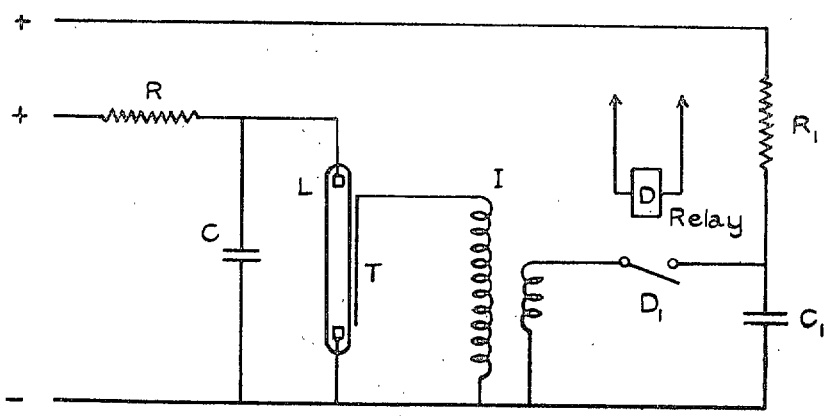

FIG. 6. Energising circuit for lamp.

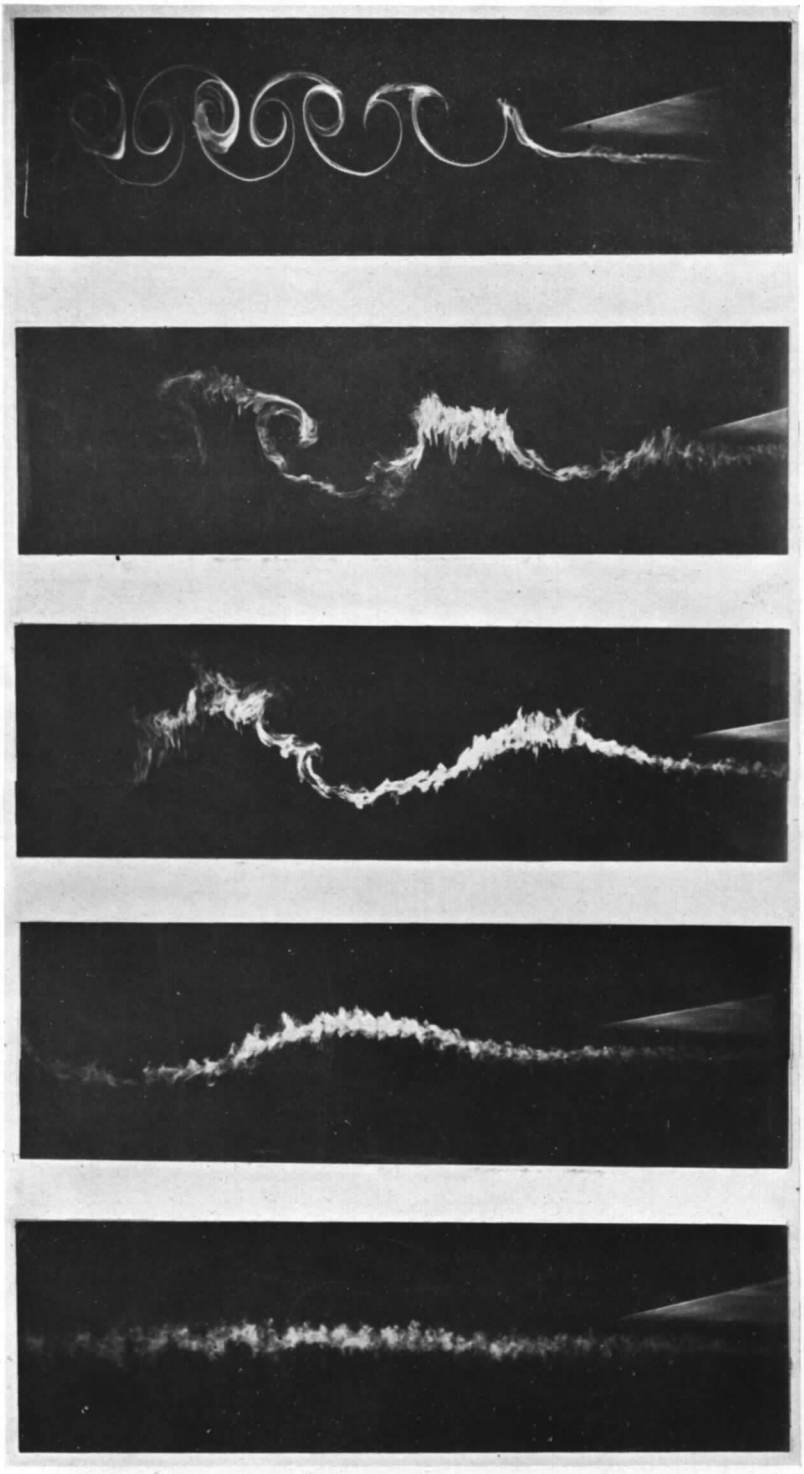

1 $f = 4 \cdot 26$ $v = 2 \cdot 6$ $\omega = 17$

2 $f = 4 \cdot 26$ $v = 8 \cdot 4$ $\omega = 5 \cdot 3$

3 $f = 4 \cdot 26$ $v = 10 \cdot 4$ $\omega = 4 \cdot 3$

4 $f = 4 \cdot 26$ $v = 12 \cdot 5$ $\omega = 3 \cdot 6$

5 $f = 4 \cdot 26$ $v = 35 \cdot 5$ $\omega = 1 \cdot 3$

FIG. 7. Variation of flow pattern with ω. Nozzle at position 1.

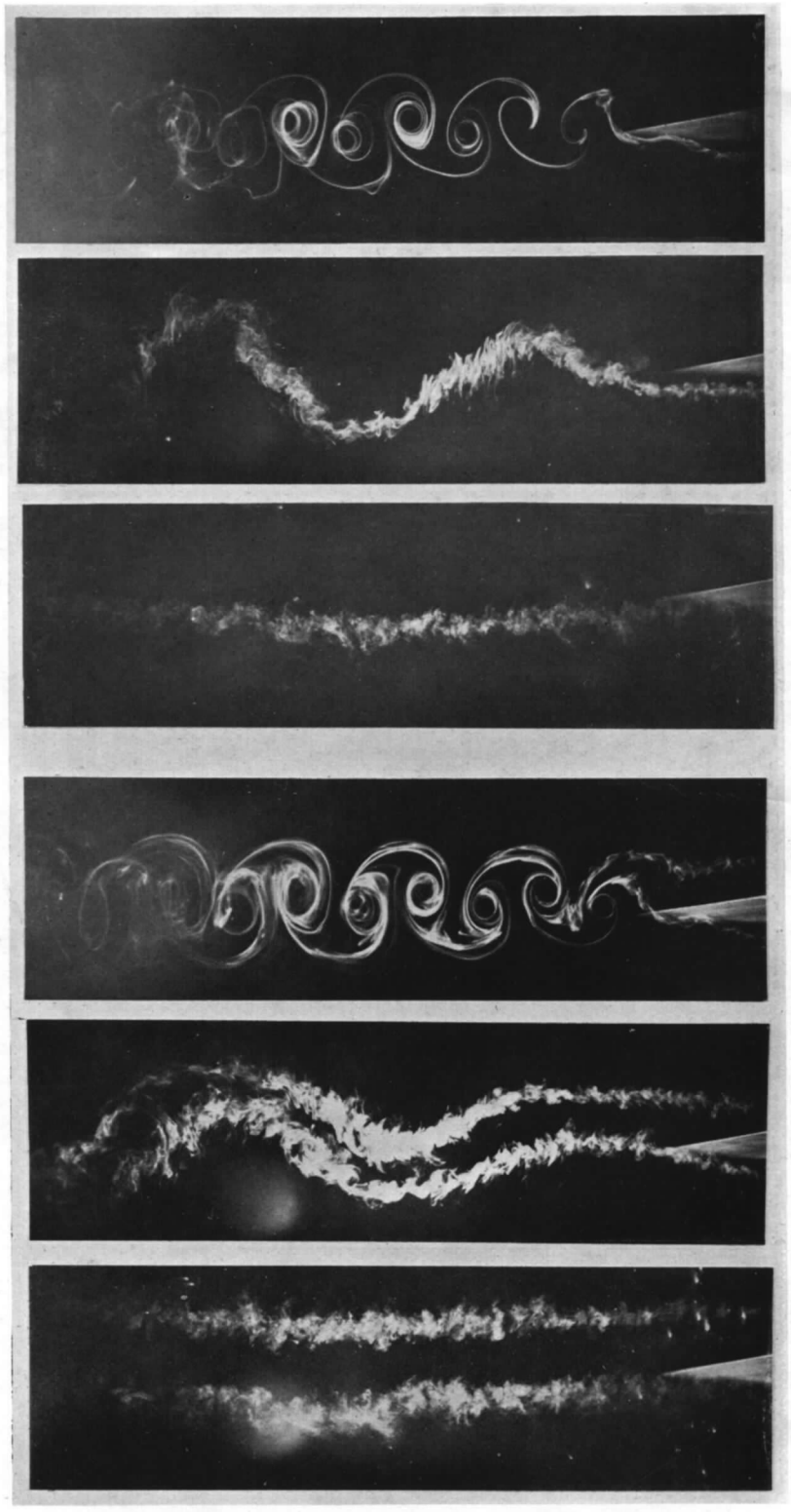

FIG. 8. Nozzles above and below level of model. Positions 2 and 3.

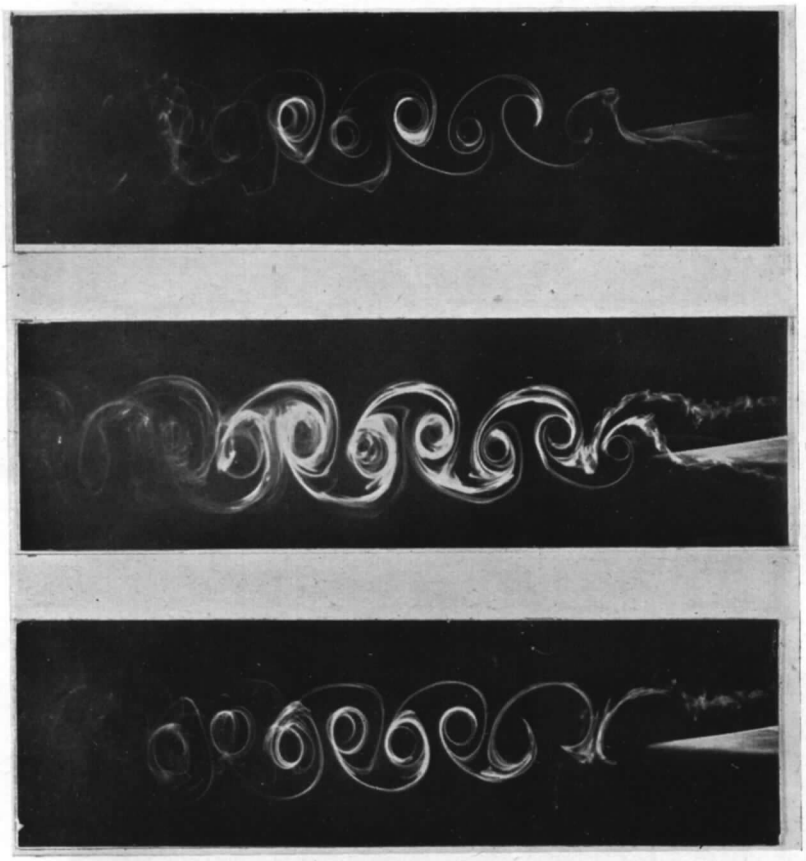

1 $f = 4 \cdot 26$ $v = 2 \cdot 6$ $\omega = 17$

2 $f = 4 \cdot 26$ $v = 2 \cdot 6$ $\omega = 17$

3 $f = 4 \cdot 26$ $v = 2 \cdot 6$ $\omega = 17$

FIG. 9. Nozzles above and below level of model. Positions 2 and 3.

$f = 0 \cdot 75$ $v = 1 \cdot 10$ $\omega = 7 \cdot 1$

FIG. 10. Flow position at low frequency and wind speed. Nozzle at position 2.

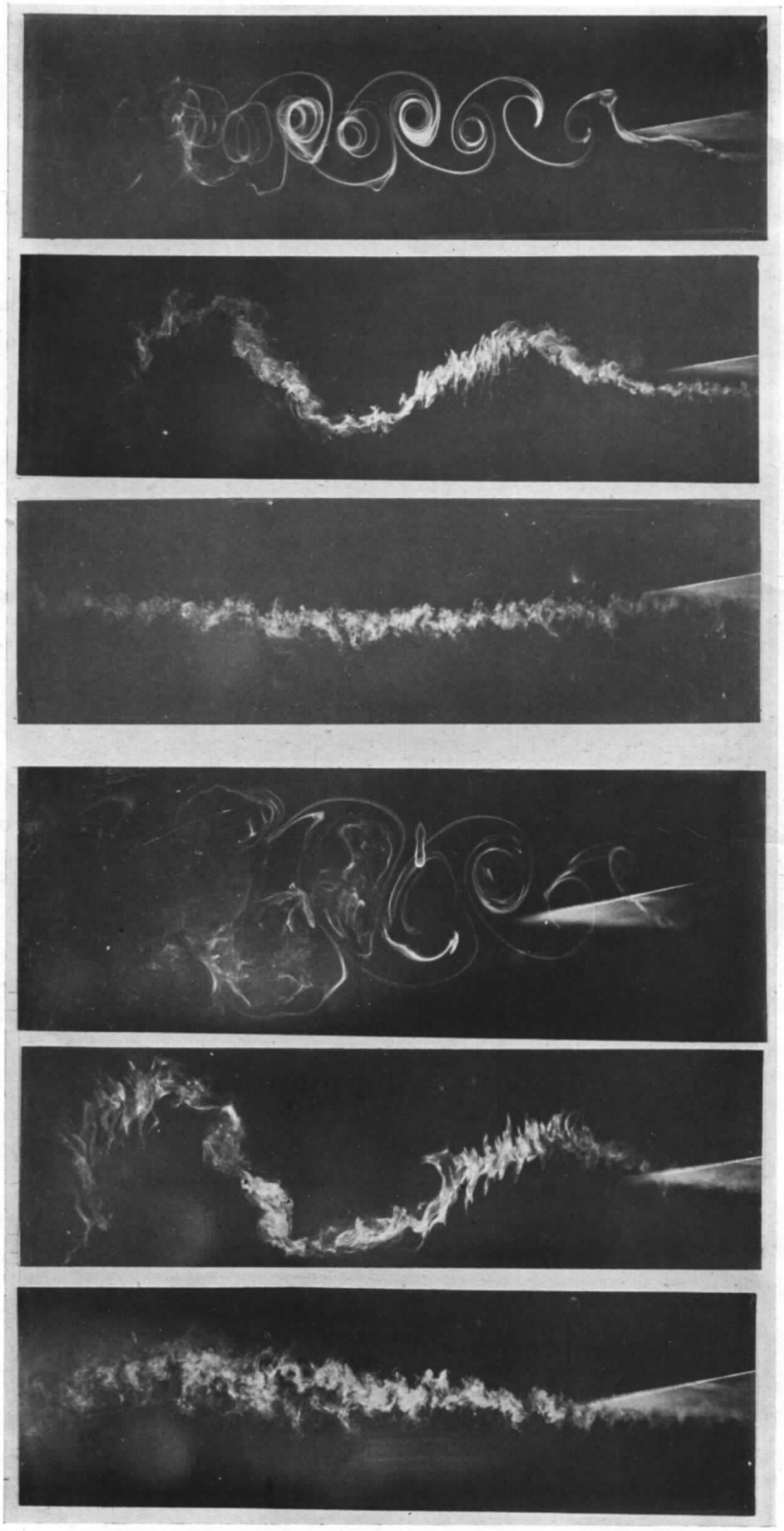

FIG. 11. Comparison of flow at two points along span.

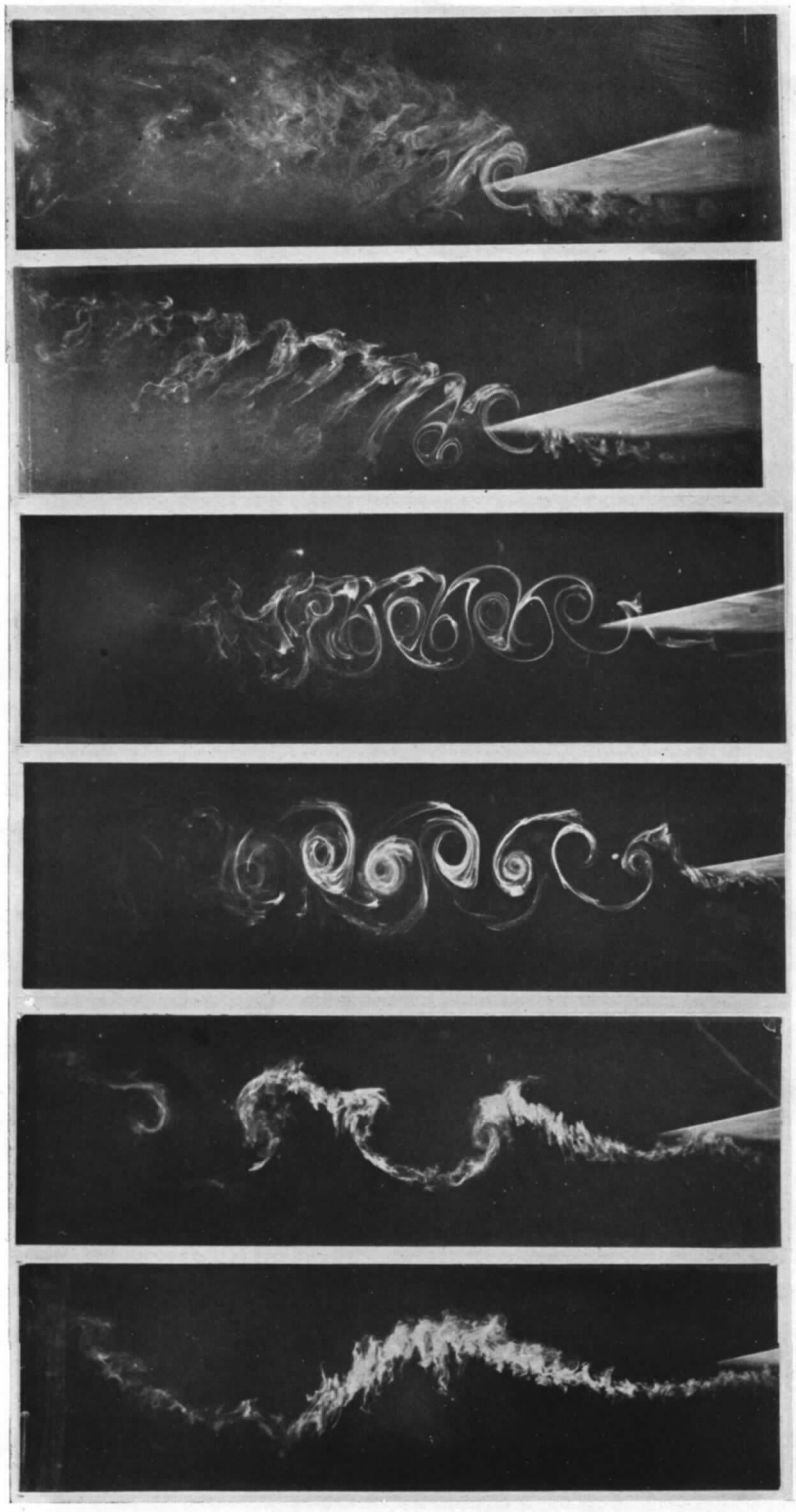

FIG. 12. Variation of flow pattern with ω. Nozzle at position 2.

FIG. 13. Comparison of flow for two values of frequency. Nozzle at position 2.

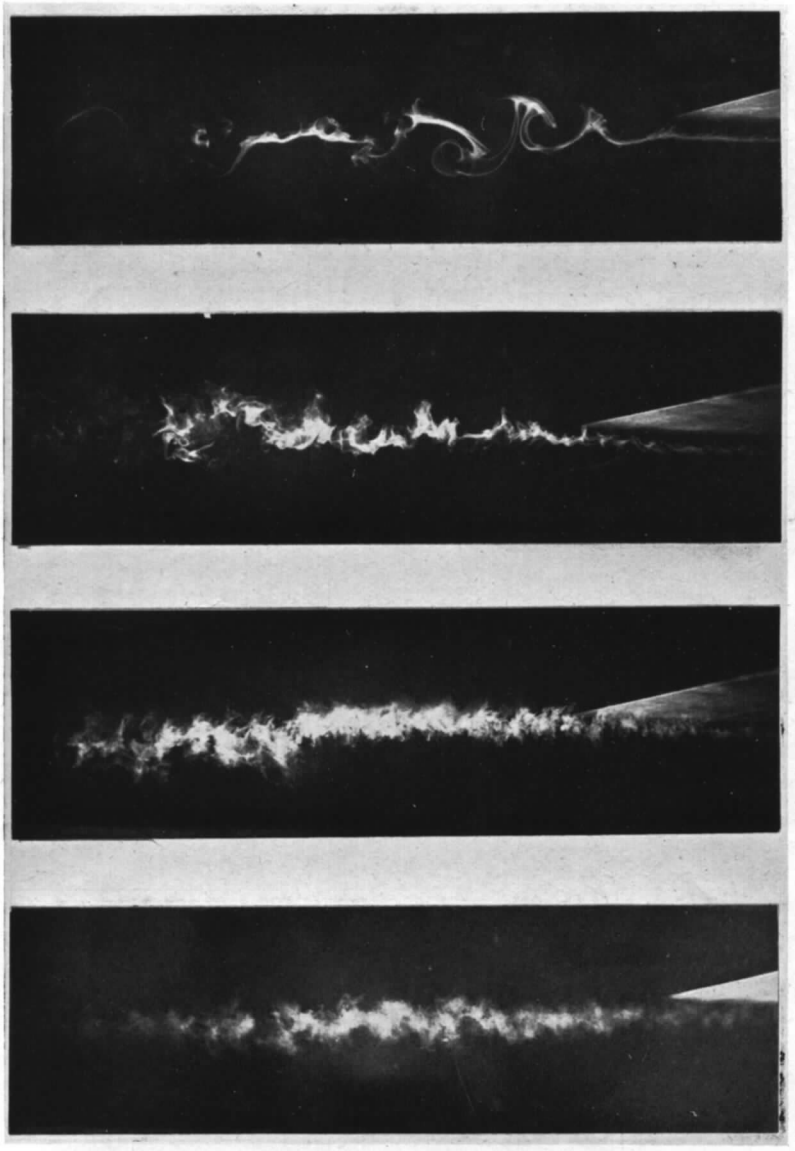

FIG. 14. Aerofoil stationary. Nozzle at position 2.

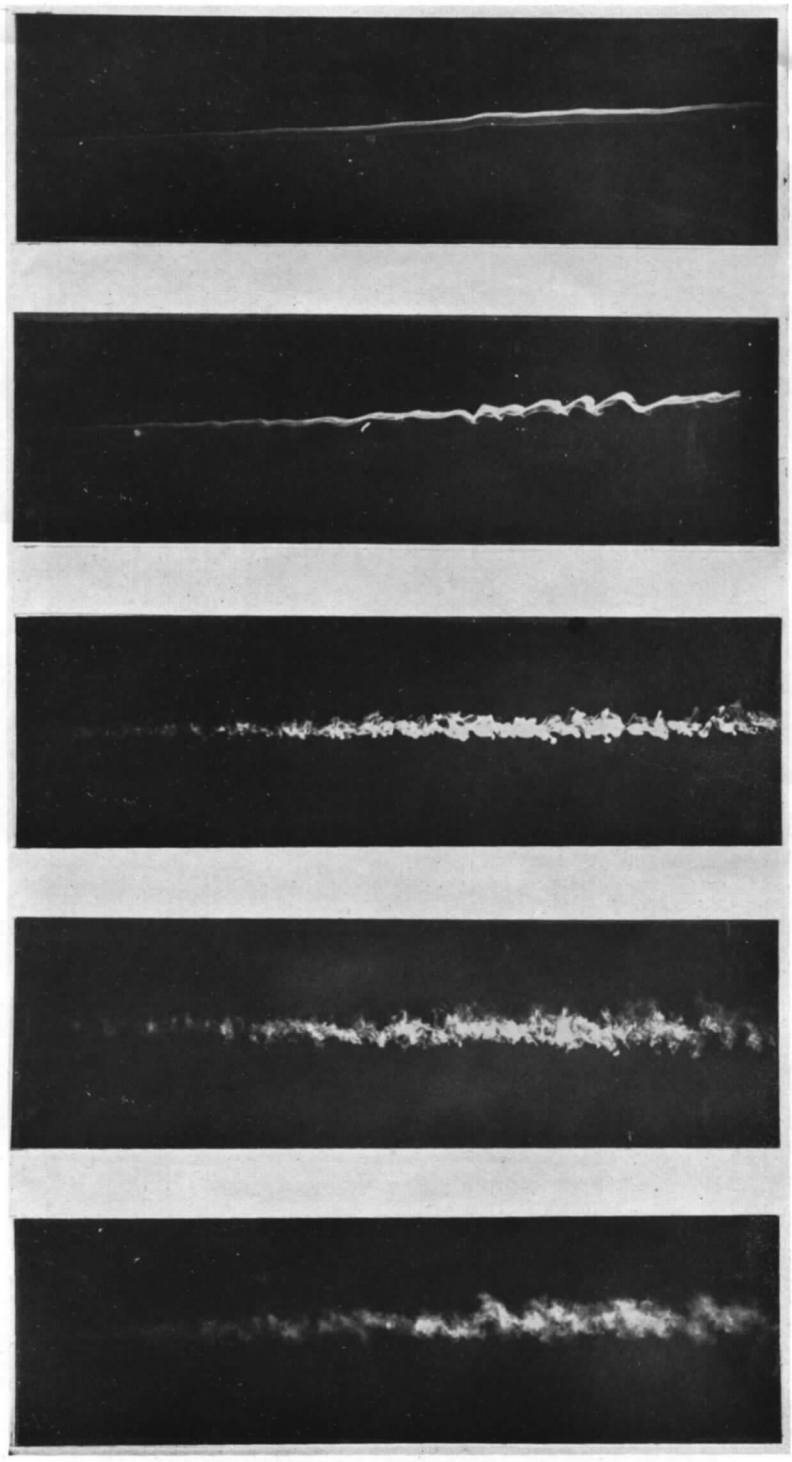

FIG. 15. Aerofoil removed from tunnel. Nozzle at position 2.

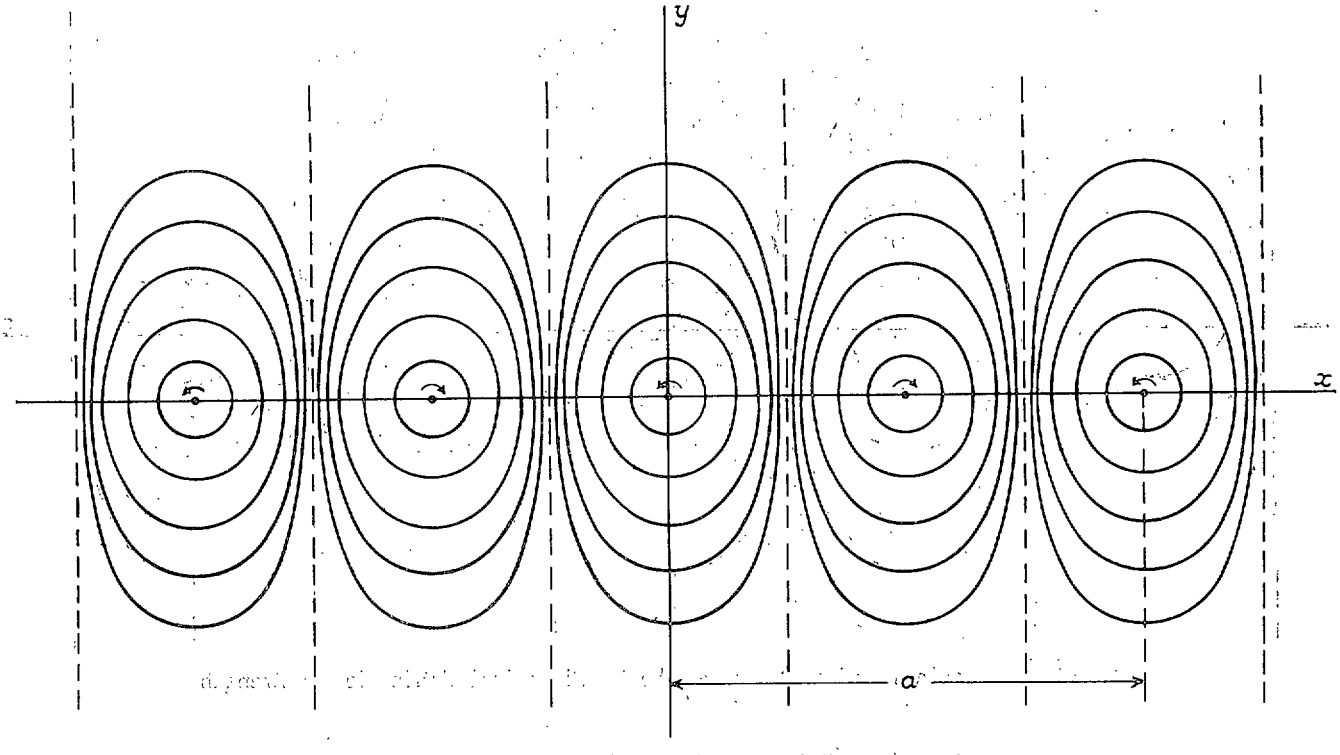

FIG. 16. Streamlines for infinite row of discrete vortices.

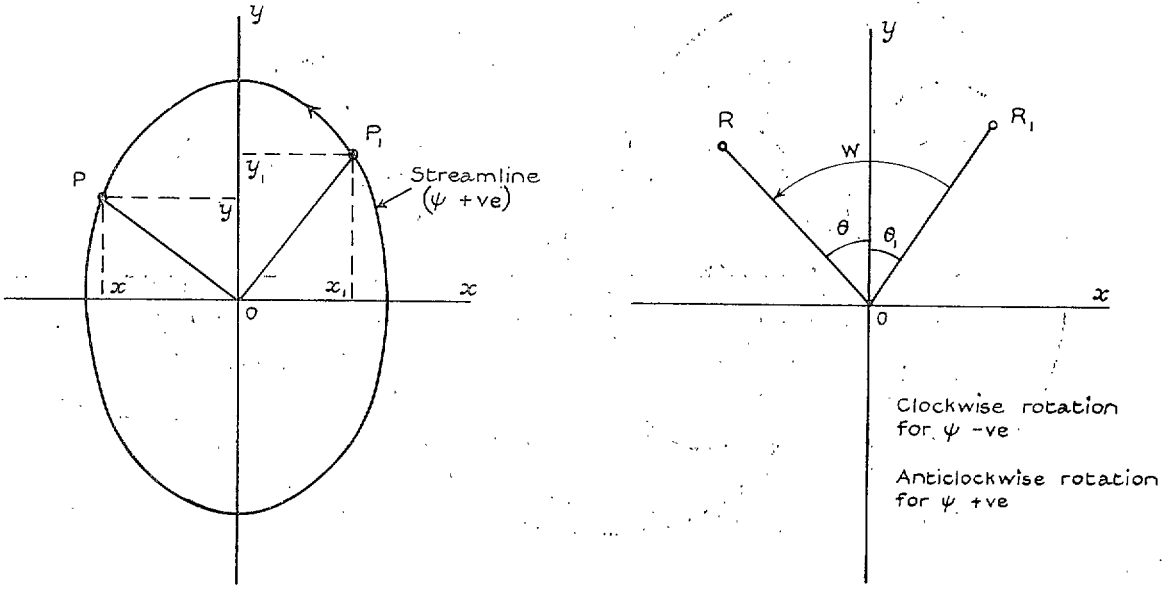

FIG. 17. Relation between θ and position on streamline. Discrete vortices.

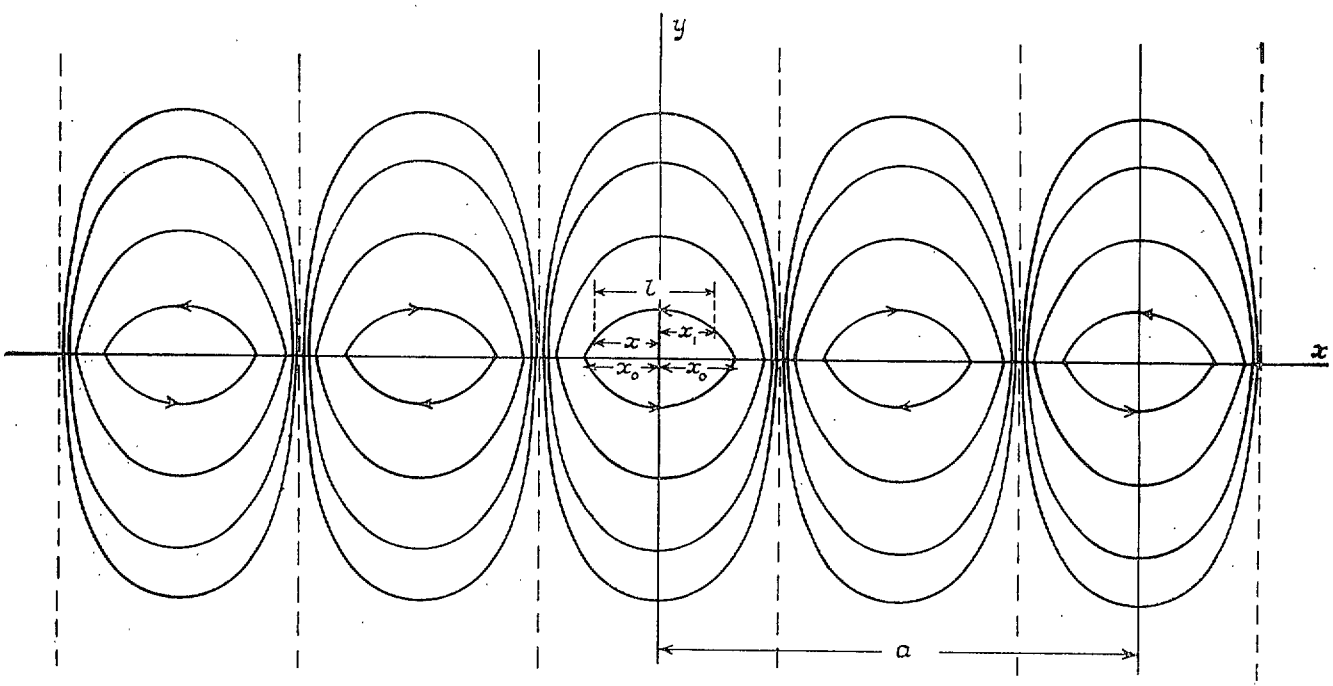

FIG. 18. Streamlines for infinite vortex sheet. Sinusoidal distribution of strength.

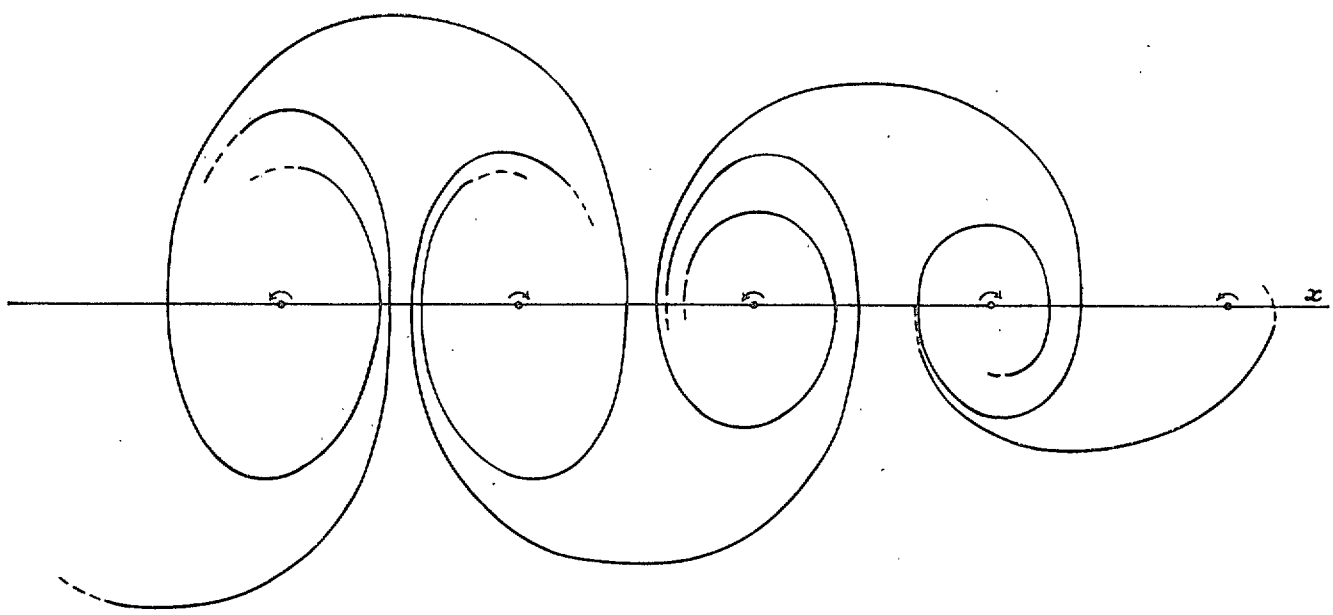

FIG. 19. Calculated smoke trace for discrete vortex system.

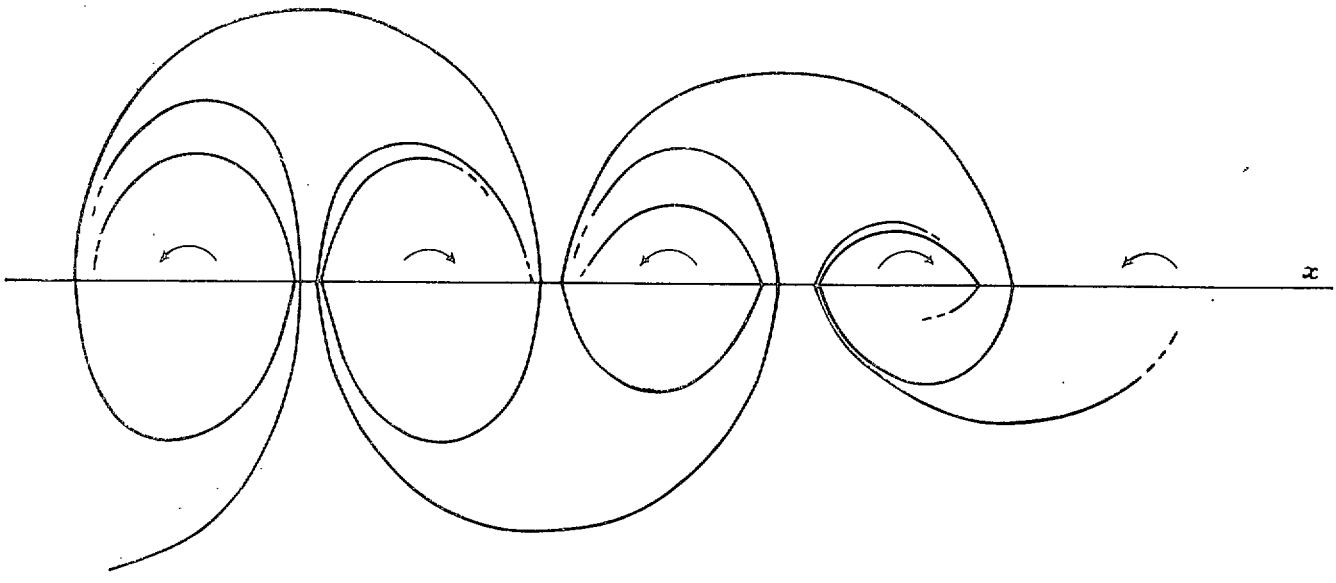

FIG. 20. Calculated smoke trace for continuous vortex system.

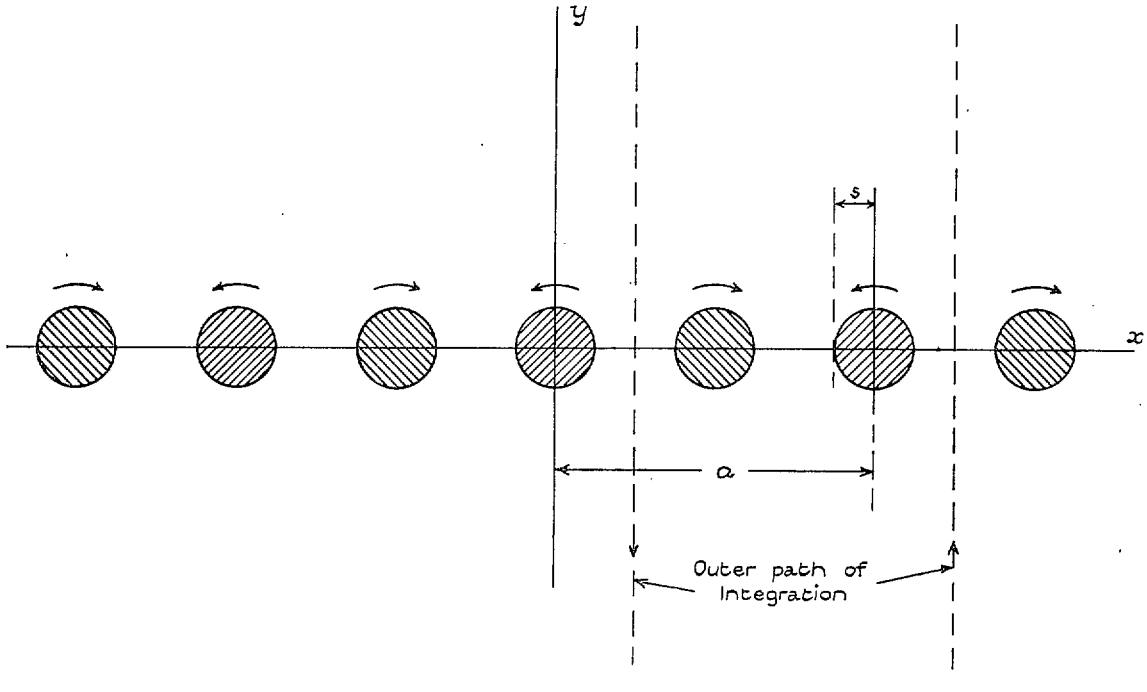

FIG. 21. Diagram of vortex cores.

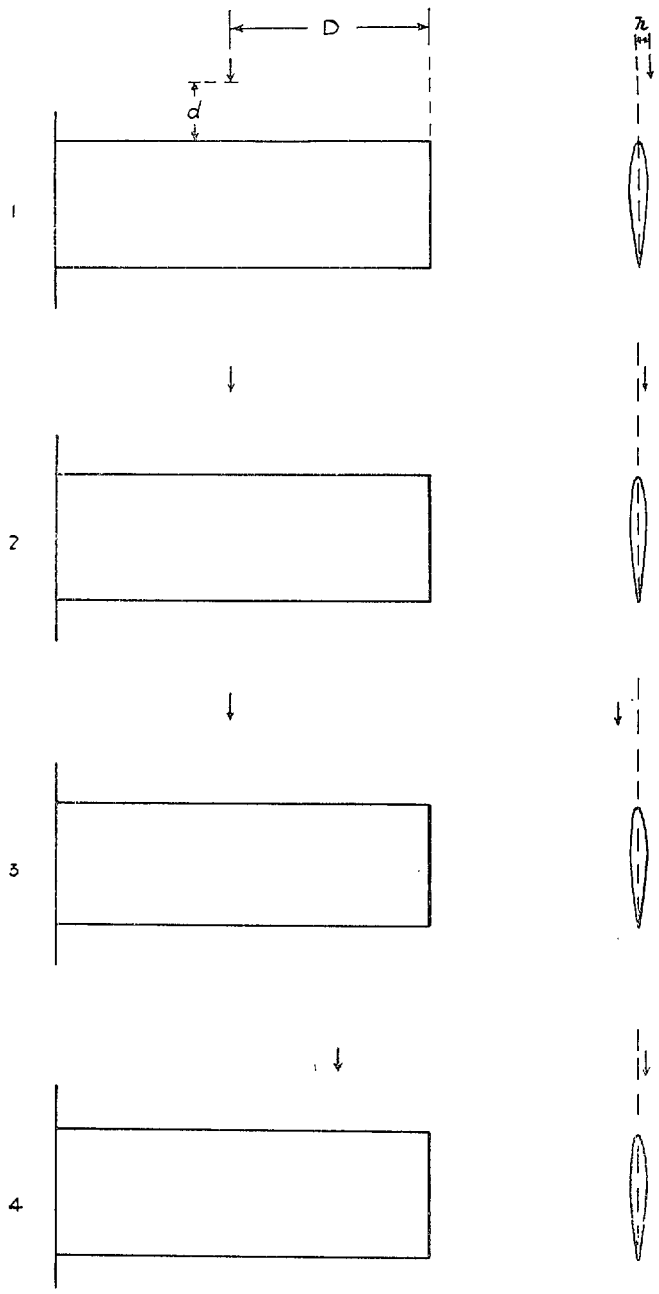

FIG. 22. Smoke nozzle positions.

(24351) Wt. 16-680 K.9 7/53 F. M. & S.

PRINTED IN GREAT BRITAIN

R. & M. No. 2773
(13,001)
A.R.C. Technical Report

Publications of the Aeronautical Research Council

ANNUAL TECHNICAL REPORTS OF THE AERONAUTICAL RESEARCH COUNCIL (BOUND VOLUMES)

1936 Vol. I. Aerodynamics General, Performance, Airscrews, Flutter and Spinning. 40*s.* (40*s.* 9*d.*)
Vol. II. Stability and Control, Structures, Seaplanes, Engines, etc. 50*s.* (50*s.* 10*d.*)

1937 Vol. I. Aerodynamics General, Performance, Airscrews, Flutter and Spinning. 40*s.* (40*s.* 10*d.*)
Vol. II. Stability and Control, Structures, Seaplanes, Engines, etc. 60*s.* (61*s.*)

1938 Vol. I. Aerodynamics General, Performance, Airscrews. 50*s.* (51*s.*)
Vol. II. Stability and Control, Flutter, Structures, Seaplanes, Wind Tunnels, Materials. 30*s.* (30*s.* 9*d.*)

1939 Vol. I. Aerodynamics General, Performance, Airscrews, Engines. 50*s.* (50*s.* 11*d.*)
Vol. II. Stability and Control, Flutter and Vibration, Instruments, Structures, Seaplanes, etc. 63*s.* (64*s.* 2*d.*)

1940 Aero and Hydrodynamics, Aerofoils, Airscrews, Engines, Flutter, Icing, Stability and Control, Structures, and a miscellaneous section. 50*s.* (51*s.*)

1941 Aero and Hydrodynamics, Aerofoils, Airscrews, Engines, Flutter, Stability and Control, Structures. 63*s.* (64*s.* 2*d.*)

1942 Vol. I. Aero and Hydrodynamics, Aerofoils, Airscrews, Engines. 75*s.* (76*s.* 3*d.*)
Vol. II. Noise, Parachutes, Stability and Control, Structures, Vibration, Wind Tunnels. 47*s.* 6*d.* (48*s.* 5*d.*)

1943 Vol. I. (In the press.)
Vol. II. (In the press.)

ANNUAL REPORTS OF THE AERONAUTICAL RESEARCH COUNCIL—

1933-34	1*s.* 6*d.* (1*s.* 8*d.*)	1937	2*s.* (2*s.* 2*d.*)
1934-35	1*s.* 6*d.* (1*s.* 8*d.*)	1938	1*s.* 6*d.* (1*s.* 8*d.*)
April 1, 1935 to Dec. 31, 1936.	4*s.* (4*s.* 4*d.*)	1939-48	3*s.* (3*s.* 2*d.*)

INDEX TO ALL REPORTS AND MEMORANDA PUBLISHED IN THE ANNUAL TECHNICAL REPORTS AND SEPARATELY—

April, 1950 - - - - - R. & M. No. 2600. 2*s.* 6*d.* (2*s.* 7½*d.*)

AUTHOR INDEX TO ALL REPORTS AND MEMORANDA OF THE AERONAUTICAL RESEARCH COUNCIL—

1909-1949 - - - - - R. & M. No. 2570. 15*s.* (15*s.* 3*d.*)

INDEXES TO THE TECHNICAL REPORTS OF THE AERONAUTICAL RESEARCH COUNCIL—

December 1, 1936—June 30, 1939.	R. & M. No. 1850.	1*s.* 3*d.* (1*s.* 4½*d.*)
July 1, 1939—June 30, 1945.	R. & M. No. 1950.	1*s.* (1*s.* 1½*d.*)
July 1, 1945—June 30, 1946.	R. & M. No. 2050.	1*s.* (1*s.* 1½*d.*)
July 1, 1946—December 31, 1946.	R. & M. No. 2150.	1*s.* 3*d.* (1*s.* 4½*d.*)
January 1, 1947—June 30, 1947.	R. & M. No. 2250.	1*s.* 3*d.* (1*s.* 4½*d.*)
July, 1951. - - - - -	R. & M. No. 2350.	1*s.* 9*d.* (1*s.* 10½*d.*)

Prices in brackets include postage.

Obtainable from

HER MAJESTY'S STATIONERY OFFICE

York House, Kingsway, London, W.C.2; 423 Oxford Street, London, W.1 (Post Orders: P.O. Box 569, London, S.E.1); 13a Castle Street, Edinburgh 2; 39 King Street, Manchester 2; 2 Edmund Street, Birmingham 3; 1 St. Andrew's Crescent, Cardiff; Tower Lane, Bristol 1; 80 Chichester Street, Belfast or through any bookseller.

S.O. Code No. 23-2773